

Relationship between Conformational Dynamics and Electron Transfer in a Desolvated Peptide. Part II. Temperature Dependence

Joel H. Parks*

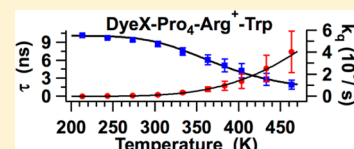
Rowland Institute at Harvard, 100 Edwin H. Land Boulevard, Cambridge, Massachusetts 02142 United States

David Semrouni, Carine Clavaguéra, and Gilles Ohanessian

Laboratoire des Mécanismes Réactionnels, Ecole Polytechnique, CNRS, 91128 Palaiseau Cedex, France

S Supporting Information

ABSTRACT: Recent time-resolved lifetime measurements studied the quenching of the fluorescence emitted by a dye covalently bound to the desolvated peptide Dye-Pro₄-Arg⁺-Trp. This peptide sequence was chosen for study since intramolecular interactions constrain all large-scale fluctuations *except* for those of the interacting dye and Trp side chain. It was shown that quenching occurred as a result of interaction between the excited dye and tryptophan side chain. These measurements exhibited a temperature dependence that suggested the quenching mechanism was related to electron transfer. This paper presents a comparison of the experimental quenching rate with the Marcus electron transfer model performed with molecular dynamics (MD) calculations. Taking advantage of the AMOEBA force field that explicitly includes polarizability ensures that the intramolecular electrostatic and polarization interactions in this desolvated peptide ion are treated realistically. MD calculations identify both large-scale fluctuations between conformations as well as small-scale fluctuations within a conformation that are shown to be correlated with torsional dynamics of the Trp side chain. Trajectories of the Dye–Trp distance identify the occurrence of close separations required for efficient electron transfer. The temperature dependence of the quenching rate closely follows the rate predicted by the Marcus electron transfer model within uncertainties resulting from statistical averages. Estimates of the energy parameters characterizing the Marcus model indicate the electronic coupling matrix element and the reaction free energy derived from the fits are consistent with published values for transfer in polyproline bridged peptides. These calculations help to provide a molecular basis for investigating conformational changes in desolvated biomolecular ions by fluorescence quenching measurements.



1. INTRODUCTION

Fluorescence-based methods have been developed to probe the structure and local conformational dynamics of trapped gas-phase biomolecular ions that have been derivatized with a strongly fluorescing dye. The motivation for these measurements was to devise a technique sensitive to conformational dynamics that could yield information about changes in intramolecular interactions. These methods have included both fluorescence resonance energy transfer (FRET) measurements and fluorescence quenching measurements. The application of FRET to oligonucleotide duplexes^{1a} as a function of temperature initially identified the transfer process by comparison of fluorescence intensity and mass spectrometry. Further FRET studies^{1b} considered fraying of the duplex structure as a function of temperature. Measurements² of fluorescence transfer between different fluorophores were performed to characterize gas phase FRET independent of biomolecule dynamics. Recently, FRET measurements³ have been performed to study the dynamics of polyproline peptides; applying measurements of both intensity and lifetime to determine the transfer efficiency at a single temperature.

The quenching of dye emission was detected initially by temperature variation of the fluorescence intensity^{4–6} and more

recently by time-resolved lifetimes.^{7,8} An early review of this research is given in ref 9. Measurements have included quenching in Trp–cage protein,^{4,6,8} polyproline peptide sequences,^{5,7} and noncovalent vancomycin–peptide complexes.⁸ Fluorescence lifetime data were found to be specifically sensitive to peptide sequence^{7,9} and intramolecular interactions.⁸ These experiments verified that interactions between the dye and a Trp residue were required to observe quenching of the dye fluorescence. In each case, the quenching rate could be related to spatial fluctuations of the side chains induced by temperature and resulting in conformational changes that increased the quenching probability.

The calculations and analyses presented in both part I¹⁰ and in this manuscript, part II, are directed toward investigating the relationship between conformational dynamics and electron transfer in a desolvated peptide. The capability to understand the quenching process on a molecular level would increase the reliability of applying these analytic methods to interpret intramolecular interactions responsible for the quenching

Received: August 7, 2012

Revised: January 2, 2013

Published: January 8, 2013

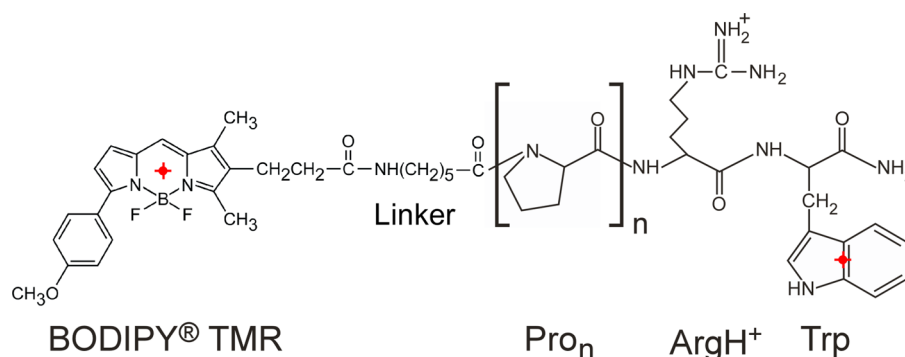


Figure 1. Chemical structure of the peptide ion DyeX-Pro_n-Arg⁺-Trp derivatized with the dye BODIPY-TMR through a dye linker. Markers (red) indicate the Dye ring center and the Trp bond center used for calculations discussed in the text.

measurements. These calculations will investigate the basis for fluorescence quenching observed in measurements⁷ of the desolvated peptide sequence DyeX-Pro₄-Arg⁺-Trp, (where X stands for a five carbon chain linker). Given the complexity of biomolecular structures, investigation of the time dependent structural fluctuations by molecular dynamics (MD) calculations provides the most reasonable approach to obtain a more comprehensive understanding of the molecular basis for the quenching process. The calculations in part I analyze conformational structures in which the dye and Trp side chain interaction is not only enhanced by fluctuations exhibiting close Dye–Trp separations, but also by parallel alignment of their ring planes. The analysis in part I identifies hydrogen bonds and electrostatic interactions that give rise to peptide conformers with high quenching probability. Part II analyzes the temperature dependence of MD trajectories associated with the fluctuating conformations. This analysis provides a comparison between the temperature dependence of the quenching rate and the dependence predicted by the Marcus model for the electron transfer rate. In addition, the calculated conformations yield an estimate of the energy of the electron transfer state that is used to determine the exothermicity of the transfer reaction. Consequently, these concerted studies provide insights into the intramolecular interactions and configurations for which the electron transfer reaction is highly probable.

The original formulation of electron transfer reactions,^{11–13} has been followed by an extensive array of theoretical studies and condensed phase experiments over the past 50 years. Particularly relevant to this paper is prior research concentrating on electron transfer in systems for which the donor and acceptor are separated by a polypeptide bridge. These studies have been shown to provide a controlled method to study the conformational dynamics driving the transfer in condensed phase measurements.^{14–16} Gas phase measurements of electron transfer in inorganic molecules have also identified the important role played by changes in conformation.^{17–21}

This paper is organized by first briefly reviewing experimental measurements of fluorescence quenching vs temperature for the peptide DyeX-Pro₄-Arg⁺-Trp. The MD calculations of conformational fluctuations of this peptide over a range of temperatures, 150–500 K, are then described and analyzed. The unique differences introduced by measurements of *desolvated* biomolecules are discussed, particularly the conformational fluctuations arising from molecular dynamics constrained by potential surface well depths $\gg kT$ resulting from electrostatic and polarization interactions within the

peptide. These analyses are then applied to comparison of the quenching rate data with the Marcus model for electron transfer. This includes (i) characterizing the Dye–Trp separation as temperature, (ii) estimating the Marcus model energy parameters, and also (iii) using trajectories to characterize the peptide intramolecular environment that helps to provide reaction exothermicity.

2. COMPUTATIONAL AND EXPERIMENTAL METHODS

2.1. Molecular Dynamics. Since quenching rates display a strong dependence on the peptide sequence, interpretation of the underlying physical process relies on an understanding of the intramolecular structure of the peptide and its dependence on temperature. MD simulations for DyeX-Pro₄-Arg⁺-Trp were performed over the temperature range of the experimental data to elucidate these peptide dynamics. Since electrostatic and many-body interactions play an important role in determining the local structures in desolvated peptides, these calculations were performed employing the AMOEBA polarizable atomic multipole force field^{22,23} as implemented in the Tinker molecular modeling software.²⁴ The AMOEBA force field provides a physical model appropriate for these desolvated peptide ions, which includes the strong electrostatic and polarization interactions between the field of the bare charge on Arg⁺ and the static and induced multipoles of both the side chains and the backbone in the peptide sequence. An example of the differences in structures derived from this force field is shown in Figure S2 of the Supporting Information and the properties of AMOEBA are discussed further in part I.¹⁰ The force field parameter set was extended to treat the Dye group by determining its atomic multipoles, using the GDMA algorithm^{25,26} based on an MP2 wave function. MD trajectory calculations were performed for each initial structure at 8 temperatures evenly distributed from 150 to 500 K. Simulations used a Berendsen thermostat and were propagated for 5 ns with a 1 fs time step and a modified Beeman integrator. Five initial structures having the lowest energies were taken from previous work⁷ and used to sample different types of low energy potential wells and thus improve statistical significance of the MD results. These five starting structures were used at each of the eight temperatures. Full technical details of these simulations can be found in part I,¹⁰ sections 2 and 3.

2.2. Experimental Section. Details of the instrumentation have been published elsewhere.^{7,9} In brief, experiments are performed on dye-derivatized biomolecular ions stored in a home-built quadrupole ion trap. The biomolecular ions are formed by nanoelectrospray (nanoES) at atmospheric pressure

and are passed through a stainless steel capillary maintained at ~ 350 K. Ions are guided into a quadrupole ion trap that is controlled over a temperature range of 150 to 465 K. The ions of interest are isolated by ejecting ions occurring at higher and lower m/z ratios. The trap electrodes and inlet for background helium gas were seated in a copper housing that was resistively heated. The trapped ions undergo $>10^5$ collisions which equilibrate them with the helium bath gas that is maintained at the temperature of the trap. Time resolved fluorescence lifetime measurements are performed by exposing the ions to 12 ps laser pulses generated by a mode-locked, diode-pumped, solid-state Nd:YVO₄ laser that excites the dye fluorescence at 532 nm. After exposure to laser excitation, ions are ejected and the mass spectrum is obtained using an electron multiplier.

3. RESULTS AND DISCUSSION

3.1. Experimental Quenching Rates. Time resolved lifetime measurements^{7–9} were performed on the (M+H)⁺ charge state of the dye derivatized peptides DyeX-Pro_{*n*}-Arg⁺-Trp ($n = 0, 4, 10$).⁷ BODIPY-TMR dye is neutral in solution and consequently Arg is the most probable protonation site. The chemical structure for this peptide is shown in Figure 1. The dye is covalently bonded to the peptide at the N terminus via a five carbon chain linker, denoted by X. Figure 2(a) displays the

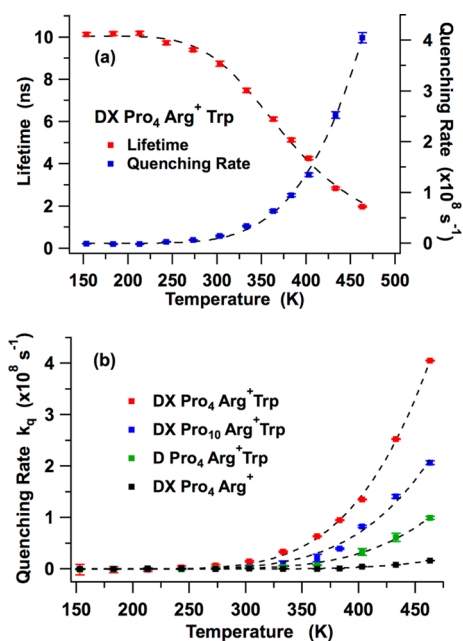


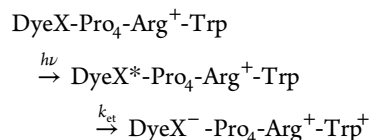
Figure 2. (a) Fluorescence lifetime (red squares) and quenching rate (blue squares) vs temperature for the protonated sequence DyeX-Pro₄-Arg⁺-Trp. (b) Comparison of the quenching rate vs temperature for protonated peptide sequences specified in the legend. Dashed lines through each set of data points are shown as guides for the eye.

lifetime and quenching rate vs temperature for the peptide sequence DyeX-Pro₄-Arg⁺-Trp. The error bars on the data represent the standard deviation of three replications of the data. The lifetime, τ , was obtained by fitting the multi-exponential fluorescent decay with a stretched exponential function. The quenching rate, k_q , is extracted from measurements of the lifetime, τ , by noting that the total decay rate of the excited state population is the sum of the radiative and quenching rates

$$\frac{1}{\tau} = \frac{1}{\tau_0} + k_q \quad (1)$$

where τ_0 is the unperturbed lifetime determined by the low temperature asymptote of τ . The lifetime data in Figure 2a asymptotes to a plateau for $T < 200$ K yielding a value for the unperturbed lifetime $\tau_0 = 10.1 \pm 0.1$ ns that is used in eq 1 to extract the quenching rate k_q . Figure 2b displays quenching rates for singly protonated polypeptide peptides designed to reduce the probability for proximity of the dye and Trp side chain. These sequences either increase the number of proline residues or eliminate the carbon chain linker with the result that the quenching rate decreases. Dashed lines are drawn through the quenching rate data for each peptide sequence shown in Figure 2 as guides for the eye. The fluorescence quenching measurements displayed in Figure 2 indicate negligible quenching in the absence of Trp, and a quenching rate for peptides containing Trp that is strongly dependent on the temperature as well as the length of the polypeptide bridge.

3.2. Molecular Dynamics Simulations. MD simulations of the peptide sequence DyeX-Pro₄-Arg⁺-Trp were performed to investigate the possibility that photoinduced electron transfer



is responsible for the observed quenching of the dye fluorescence. MD calculations and analyses of the DyeX-Pro₄-Arg⁺-Trp structures will concentrate on two primary questions. How do the conformations and conformational fluctuations for this peptide evolve with increasing temperature to produce a monotonically increasing quenching rate? How are these peptide conformations incorporated into a quenching model based on electron transfer? This model not only is required to reproduce the measured temperature dependence, but also needs to yield energy parameters consistent with previous solution phase measurements of electron transfer across polypeptide bridges.

(a). Peptide Sequence Design. The peptide sequence, DyeX-Pro₄-Arg⁺-Trp, was designed with the expectation that the ring structure in the proline side chain would constrain large fluctuations of the polypeptide chain.^{27,28} Figure S3 in the Supporting Information shows superimposed structures of the peptide calculated at 250 and 500 K for 10 trajectory times taken at 0.5 ns intervals. These superimposed structures were created using UCSF Chimera molecular graphics and analysis software.^{29,30} Chimera routines were used to generate sequence alignments and graphics of the two superimposed groups of structures shown in the Supporting Information, Figure S3. The structures at both temperatures exhibit large-scale fluctuations resulting in RMSD = 0.283 Å at 250 K and RMSD = 0.874 Å at 500 K. In Figure S3, Supporting Information, the arginine and proline residues exhibit only small-scale fluctuations at both temperatures compared to the dye and tryptophan dynamics that are dominated by significantly larger fluctuations.

This result is shown more quantitatively by calculating the radial average position, $\langle r \rangle$, and standard deviation, σ_r , for the dye and each residue. These values are obtained from averages over trajectories of $\langle r_i \rangle = \langle (x_i^2 + y_i^2 + z_i^2)^{1/2} \rangle$ in which i indicates coordinates of the center of mass (CM) of the BODIPY-TMR rings and the central bond position of the Trp

rings (indicated in Figure 1), the carbon in the Arg guanidinium group, and the C_α positions of the Pro residues. The ratio $\sigma_r / \langle r \rangle$ characterizes the scale of the fluctuations for the dye and each residue. As shown in Table 1, this ratio is an

Table 1. Side Chain Fluctuations^a

<i>T</i> , K	dye ^b	Trp ^b	Arg ^c	Pro1 ^d	Pro2 ^d	Pro3 ^d	Pro4 ^d
250	0.120	0.130	0.034	0.012	0.015	0.018	0.012
500	0.150	0.170	0.045	0.017	0.051	0.062	0.064

^aEach entry is the ratio $\sigma_r / \langle r \rangle$ described in the text. ^bCoordinate position shown in Figure 1 ^cCoordinate of C atom in Arg guanidinium group. ^dCoordinate of C_α atom in each Pro residue.

order of magnitude larger for the dye and Trp than for Arg and Pro residues. The semirigid behavior of the polyproline chain is expected and results from the steric hindrances introduced by the ring structures of the proline side chains.³⁰ However, the stability of the arginine side chain against large fluctuations was shown in part I¹⁰ to result from the presence of hydrogen bonds. Consequently, studies with this peptide sequence essentially reduces the structural dynamics to a study of the dye and Trp fluctuations, greatly simplifying analysis to relate conformational fluctuations to the quenching process.

(b). *Collective Motions in DyeX-Pro₄-Arg⁺-Trp*. The analysis of protein fluctuations “can be separated into local oscillations superposed on motions with a more collective character”.³¹ Whereas the former are associated with the motions of individual atoms occurring on the subpicosecond time scale, the latter relate to correlated motions of many atoms on the 1–10 ps time scale. These dynamics include rigid body motions, such as torsions, of the backbone and residue side chains, in particular of the Trp side chain and the dye molecule in the peptide under study

The trajectories shown in Figure 3 display fluctuations of the Dye–Trp separation as changes in their center-to-center separation defined in Figure 1. Figure 3 shows trajectories calculated for each starting structure at temperatures 250 and 400 K. These trajectories exhibit sections of rapid atomic fluctuations superimposed on relatively long plateaus at specific Dye–Trp separations. These plateaus result from larger fluctuations of the Dye and Trp molecules that are shown in Figure 3 to form similar conformer structures for relatively long times during which we assume they are trapped within local minimum on the potential energy surface. On average, the frequency of these plateaus increases and their duration decreases with increasing temperature, consistent with overcoming potential barriers that stabilized the conformer structure. However, it is important to try to identify the specific dynamics leading to the trajectory plateaus observed in Figure 3 and thus determine how they are related to collective motions.

Previous studies have investigated conformational dynamics depending on torsional motions of tryptophan and CH_2 chains. We briefly review those results prior to a discussion of torsional dynamics in the DyeX-Pro₄-Arg⁺-Trp peptide.

Myoglobin. Henry and Hochstrasser performed fluorescence resonant energy transfer (FRET) measurements³² to investigate the rate that energy was transferred from tryptophan residues to the heme group in myoglobin. MD simulations performed to calculate the Förster energy transfer rate were found to adequately predict the observed heme fluorescence decay. The MD trajectories of the two tryptophan residues in myoglobin indicated that the side chains undergo both small, rapid orientational fluctuations and large infrequent transitions between different torsional isomers. These dynamics were assigned to torsional motion about the (C_α – C_β) bond that

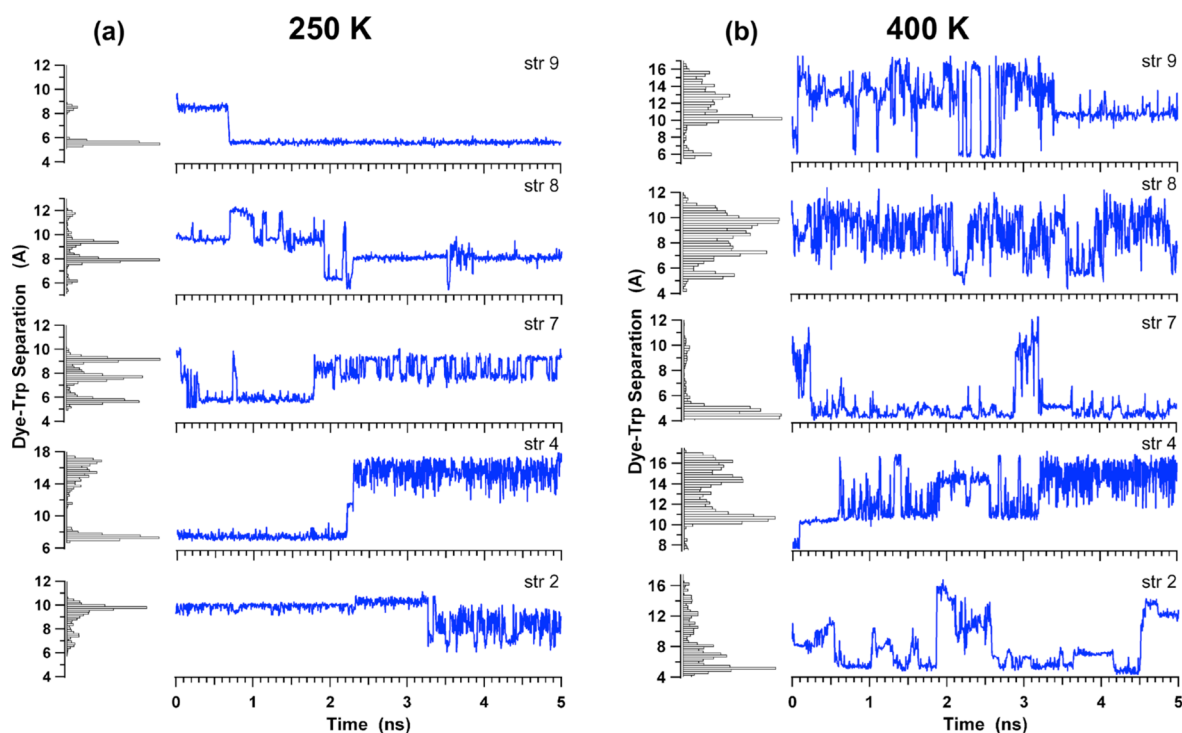


Figure 3. Molecular dynamics trajectories and associated histograms of center-to-center Dye–Trp separation for each of the 5 starting structures at temperatures (a) 250 K and (b) 400 K.

produced changes in the myoglobin Trp–heme separation as large as 2–3 Å.

Tryptophan. The electronic state spectroscopy of neutral tryptophan in the gas phase has been performed using resonant enhanced two-photon ionization on supersonic jet-cooled molecular beams that allowed the study of individual conformers.³³ Spectra of resonant two-photon ionization as well as dispersed tryptophan fluorescence³⁴ identified that the lowest energy conformer exhibits a nearly harmonic 26 cm^{-1} vibrational progression associated with the ground state potential surface. The absence of this low frequency progression in the spectrum of indole^{35,36} or 3-methylindole,^{35,37} indicated that these vibrations involved bonds linking the side chain to the backbone segment of tryptophan. This low frequency vibrational progression in the lowest energy tryptophan conformer was also observed in cavity ring-down absorption and laser-induced fluorescence spectra.³⁸ Density functional calculations³⁸ that optimized the geometry of tryptophan torsional conformers and their vibrational modes confirmed that the observed low frequency progression is consistent with a torsional motion of the tryptophan side chain about the (C_β – C_γ) bond.

CH_2 Chains. Torsional modes associated with C–C bonds have been identified for a methylene bridge (CH_2)₃ linking two aromatic chromophores.^{18,19} Torsional motions of the bridge enabled interaction of the chromophores leading to gas phase electron transfer. The fluorescence emission spectra identified a vibrational progression having a fundamental frequency of 11 cm^{-1} . Supporting calculations estimated these spectral components resulted from torsional modes with frequencies in the range 8 – 27 cm^{-1} .

DyeX-Pro₄-Arg⁺-Trp. In order to study the correlation between the Trp side chain fluctuations and the Dye–Trp proximity in this peptide, we have followed the evolution of the Trp side chain dihedrals X_1 and X_2 defined as: $\text{N-C}_\alpha\text{-C}_\beta\text{-C}_\gamma$ and $\text{C}_\alpha\text{-C}_\beta\text{-C}_\gamma\text{-C}_{\delta 1}$ respectively. In this notation, the dihedral angle X_1 denotes rotation about the (C_α – C_β) bond and X_2 rotation about the (C_β – C_γ) bond. The carbon atoms specified by C_γ and $C_{\delta 1}$ are positioned in the indole ring. The instantaneous values of these dihedrals were calculated every 0.1 ps (100 steps).

Figure 4 displays correlations between the trajectories for the torsional dihedral angles and Dye–Trp separations. Examples at lower temperatures have been chosen to reduce the congestion of conformational changes so that the correlations are not obscured. Figure 4a for str9 at 250 K displays the simplest correlation in which a single decrease in Dye–Trp of ~ 8.5 to 5.5 Å is related to a change in X_1 of $\sim 60^\circ$ to -180° . In this case, X_2 exhibits only rapid, small orientational fluctuations about $\sim 90^\circ$ but does not contribute significantly to the change in proximity. Figure 4b, for str9 at 300 K demonstrates how rapidly the situation can change with increasing temperature. Note that both dihedral angles are now active: with X_2 changing from $\sim 90^\circ$ to -60° during the large Dye–Trp change of $\sim 10\text{ Å}$ to 5 Å yielding a plateau at close proximity for $\sim 1.25\text{ ns}$. Although a decrease in X_2 signals the increase in Dye–Trp proximity, return to a larger separation apparently is related to a decrease in X_1 . Figure 4c for str7 at 250 K shows similar correlated dynamics involved in plateau formation for 0 to $\sim 1.8\text{ ns}$; however, a different dynamic is observed for times $>1.8\text{ ns}$. During the latter part of the X_1 trajectory, the dihedral angle exhibits a continuing, random vacillation between $+30^\circ$ and -60° that is clearly expressed in the dynamics of the Dye–Trp

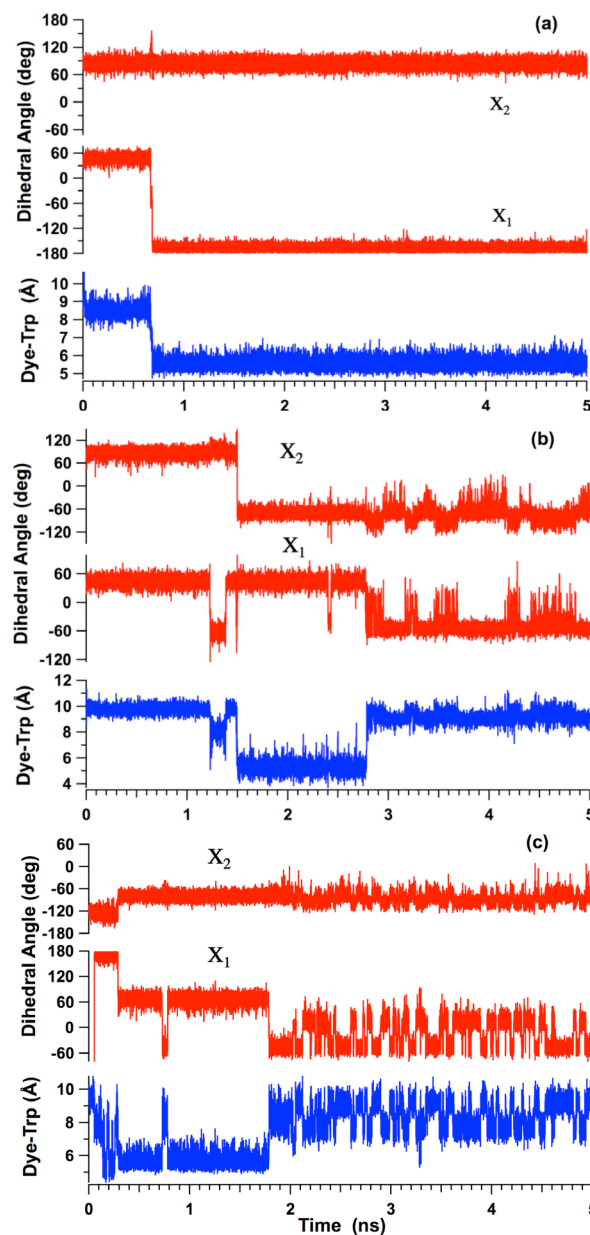


Figure 4. Molecular dynamics trajectories of (a) str9 at 250 K, (b) str9 at 300 K, and (c) str7 at 250 K. Dihedral angles X_1 and X_2 are shown in red, Dye–Trp separation is shown in blue.

separation. In this case, the proximity variation occurs with the opposite phase.

The correlated dynamics that are evident in Figure 4 are consistent with the conclusions from studies of myoglobin³⁹ that for temperatures above 180 K, the peptide dynamics are expected to be torsional fluctuations. However, the Trp torsions are probably only part of the contributions to Dye–Trp separation for higher temperatures. Not only are wider regions of the potential surface sampled, but also additional dynamical contributions are present. In addition to the torsional mode fluctuations about bonds in the tryptophan side chain shown in Figure 4, dynamic contributions also are expected to occur for the Dye linker, the arginine side chain and possibly backbone motion. For example, the conformational change occurring near 1.8 ns in Figure 5 indicates changes in position of both the Trp and Arg side chains

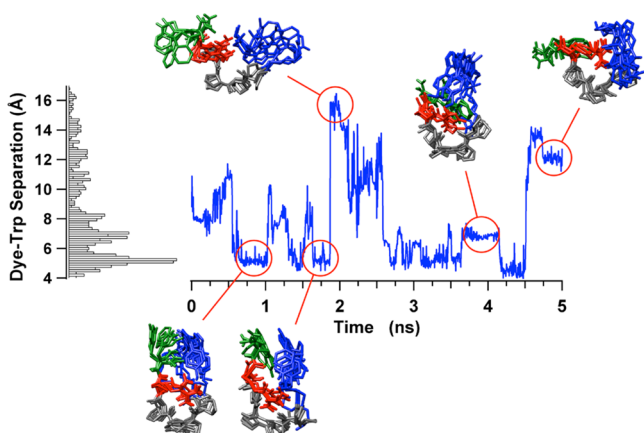


Figure 5. Molecular dynamics trajectory and associated histogram of center-to-center Dye–Trp separation for starting structure 2 at 400 K. Overlapping structures characterizing peptide conformations in several plateau regions are shown and described in the text.

resulting in increased flexibility of both the Dye and Trp. The dye also can undergo positional changes as the result of torsional fluctuations about the C–C bonds of the carbon chain of $(\text{CH}_2)_5$ coupling the dye to the peptide N terminus. In general, the dynamics at higher temperatures are not simply correlated with the X_1 and X_2 torsions of the Trp side chain indicating that such changes involve contributions from a larger group of trajectories.

(c). *Transitions among Peptide Conformations.* The histograms associated with trajectories at 250 K in Figure 3a indicate fluctuations dominated by relatively few, large, narrow histogram peaks, consistent with conformations trapped in potential minima of depth $\gg kT$. Trajectories at 400 K in Figure 3b exhibit histograms having broad bands corresponding to increased motion on the potential surface, but continue to exhibit narrow peaks associated with trapping in potential minima deeper than kT . The increase in thermal energy enables the peptide to sample extended areas of the potential energy surface; however, the probability also increases for the peptide to find and become localized in minima associated with Dye–Trp proximity. The sharp histogram peaks for Dye–Trp separations ≥ 6 Å are probably associated with longer range electrostatic interactions, and those peaks closer to 4 Å with van der Waals interactions as identified in part I.¹⁰ It is clear from Figure 3 that the rate of large fluctuations varies with starting structure and indicates no evidence of convergence to a common structure within 5 ns. Note that the MD time scale is within a factor of 2 of the experimental time scale set by the unperturbed lifetime of 10 ns and is greater than the quenched lifetimes. Consequently, fluctuations among the calculated plateau conformations are probably close to the dynamics probed by the dye during photon interactions. The trajectories shown in Figure 3 are consistent with dynamics on a potential energy surface that is sufficiently constrained by interactions that the surface region sampled by the peptide remains relatively local, retaining characteristics of the starting structure.

Trajectories of the Dye–Trp separations in Figure 5 at 400 K for starting structure 2 are composed of large transitions of up to 10 Å between plateaus of small scale fluctuations lasting from ~ 0.1 –1 ns. In the discussion above, we suggested that these large-scale fluctuations represent *transitions between conformations* and the small-scale fluctuations occur within a specific conformation. The Dye–Trp trajectory in Figure 5 illustrates

this dynamic behavior in images formed by 4 overlapping structures chosen at different times within the indicated plateaus. Each group of plateau structures exhibits a set of similar conformations to within the small-scale structure fluctuations. Note that the two groups of structures having Dye–Trp separations of ~ 5 Å exhibit similar structures; whereas the remaining three groups with significantly different separations have very dissimilar conformations.

The MD and DFT analyses of DyeX-Pro₄-Arg⁺-Trp structures presented in part I¹⁰ compared the decomposition of the interaction energies with the Dye–Trp separation and also the dihedral angle between the planes of the dye and Trp ring structures. These analyses conclude that electrostatic interactions and polarization play an important role in the sharp conformational transitions observed in Figure 5. Understanding the basic process responsible for the quenching reaction is necessary to discern how the peptide dynamics are related to the quenching rates. Is it simply that the electrostatics and polarization interactions lead to conformers with small Dye–Trp separations that are required for fast rates, or in addition, do these interactions also enhance the rates through other processes? In either case, the experimental data⁷ clearly indicated that both the Dye–Trp separations as well as electrostatics play a role in determining the quenching rate. The following sections will present a model for the temperature dependence of electron transfer and will apply the model to describe the fluorescence quenching rates for the DyeX-Pro₄-Arg⁺-Trp peptide. In addition, a basis for the quenching rate dependence on electrostatics and polarization interactions will be presented.

4. COMPARISON OF QUENCHING RATE DATA WITH ELECTRON TRANSFER RATES

4.1. Electron Transfer Model. (a). *Marcus Model: Temperature Dependence.* The Marcus formulation for the rate of electron transfer^{11–13} is expressed by Fermi's golden rule applied to a nonadiabatic reaction between reactant and product states

$$k_{\text{et}} = \frac{2\pi}{\hbar} H_{12}^2 \rho_{\text{FC}} \quad (2)$$

where

$$\begin{aligned} \rho_{\text{FC}} &= \frac{1}{\sqrt{4\pi\lambda k_B T}} \exp\left\{-\frac{(\Delta G + \lambda)^2}{4\lambda k_B T}\right\} \\ &= \frac{1}{\sqrt{4\pi\lambda k_B T}} \exp(-\Delta G_{\text{act}}/k_B T) \end{aligned} \quad (3)$$

is the Franck–Condon weighted-density of states formed from the overlap of reactant and product nuclear wave functions. This is derived using classical harmonic oscillator wave functions with identical frequencies, ν , in the high temperature limit for which the temperature T satisfies $k_B T \gg \hbar\nu$, where k_B is the Boltzmann constant. As discussed above in section 3.2(c), the collective motions in the trajectories of the Dye–Trp separation that are important for electron transfer are probably occurring in the dynamics of the low frequency torsional modes, ν_T . In this case, the condition $k_B T \gg \hbar\nu_T$ for the Marcus transfer rate given above is well satisfied over the experimental temperature range by the torsion modes for which $(\nu_T/c) \sim 10$ –30 cm^{-1} . This justifies treating the vibrations classically in the Marcus model of electron transfer for analysis

of the temperature dependence of the quenching rate data shown in Figure 2a. The reorganization energy λ is the energy required to transform bond lengths and angles of the reactant state into their values at equilibrium geometry of the product state. The free energy difference, $-\Delta G = (G_R - G_P)$, between reactant (R) and product (P) electronic states is the exothermicity driving the transfer reaction when $G_R > G_P$. The activation energy for electron transfer is approximated by

$$\Delta G_{\text{act}} = \frac{(\Delta G + \lambda)^2}{4\lambda} \quad (4a)$$

and

$$H_{12}^2 = V_{12}^2 \exp(-\beta r_{A-D}) \quad (4b)$$

is the matrix element of the energy coupling the reactant and product electronic wave functions. This matrix element expresses the wave function overlap as an exponential decay with distance in eq 4b, where $r_{A-D} = r_{\text{Dye-Trp}}$ is the distance between electron donor Trp and the acceptor Dye, and β (\AA^{-1}) is the decay coefficient. Equation 2 describes nonadiabatic electron transfer^{13,40} that occurs under conditions for which $H_{12} \ll k_B T$, for example large donor–acceptor separations or a small value of V_{12} . It is not obvious that electron transfer in the peptide under discussion satisfies conditions for a nonadiabatic process and this will be discussed further in section 4.2(e).

In the Marcus model of nonadiabatic electron transfer, the rate is determined by three key quantities: reorganization free energy, λ ; free energy difference, ΔG ; and the electronic coupling energy, H_{12} . Figure 6 illustrates a potential energy

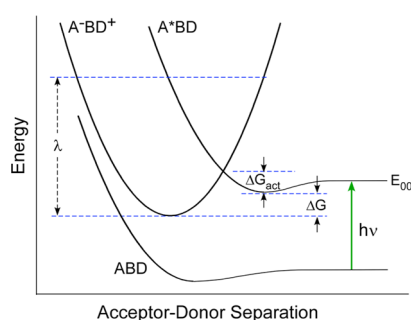


Figure 6. Potential curves describing the ground (ABD), locally excited (A^*BD), and electron-transfer (A^-BD^+) states of the peptide studied in this paper, where A, B, and D stand for acceptor, bridge and donor, respectively. Plotted along the x axis is the distance between the Dye and Trp residue. This model depicts excitation from a van der Waals ground state to an exciplex state indicated by the green arrow. The electron-transfer state lies below the locally excited state at the electron-transfer state minimum but above the locally excited state at the excited state minimum. The various energies indicated for the potential curves are described in the text.

diagram of nonadiabatic states in which a ground state (ABD) is a weakly bound state formed during conformational fluctuations which becomes an exciplex reactant state (A^*BD) after laser excitation of the attached dye. The notation indicates that the donor (D) and acceptor (A) moieties are separated by a bridging sequence (B). The product state (A^-BD^+) in Figure 6 is shown crossing the exciplex reactant state and the associated energy parameters λ , ΔG and ΔG_{act} are defined on the potential diagram. For the peptide under consideration, the sequence in the reactant state is $\text{DyeX}^-[\text{Pro}_4\text{Arg}^+]\text{Trp}$ and in the product state is $\text{DyeX}^-[\text{Pro}_4\text{Arg}^+]$.

Trp^+ . The discussion in section 3.2(a) has emphasized that the bridging residues $[\text{Pro}_4\text{Arg}^+]$ remain relatively stable against large spatial fluctuations over the temperature range of the MD calculations.

Electron transfer in the Marcus model occurs during an encounter between the donor and an acceptor that is sufficiently close to form a weak overlap of their wave functions. Fluctuations of surrounding solvent molecules occurring during this atomic configuration interact with the donor and acceptor electronic states through low-frequency solvent vibrational modes. These interactions help to form the electronic configurations of intermediate states having high probability for electron transfer. Jortner provided a quantum mechanical treatment⁴¹ of electron transfer that identified the importance of contributions by higher frequency molecular modes on the transfer dynamics. In particular, Jortner provided a derivation of the temperature dependence of the transfer rate for biomolecules that reduces to the Marcus formulation in the high temperature limit. This quantum treatment was extended^{20,42} to consider the conditions for occurrence of electron transfer in an *isolated solvent-free* biomolecule. Jortner identifies alternative intramolecular interactions involving high frequency vibrational modes that introduce the electronic-vibrational coupling required for reorganization to form the intermediate states. It is also pointed out,⁴² that desolvated, *flexible* organic molecules¹⁸ can introduce intramolecular electronic interactions involving low frequency modes that can couple the donor and acceptor electronic states. In these cases, intramolecular vibrations effectively replace the solvent degrees of freedom and the presence of solvent modes is not required for charge transfer.

Desolvated, flexible biomolecules that have been protonated during the electrospray process such as the $\text{DyeX-Pro}_4\text{Arg}^+\text{Trp}$ peptide introduce yet additional interactions and conformational dynamics leading to the configurations having high probability for electron transfer. In the compact conformations identified for this peptide in part I,¹⁰ the Dye and Trp reside within a highly polarizable medium formed by the remaining residues. An important consequence of this surrounding medium is the coupling of electronic states with the low frequency modes of the peptide conformation. This coupling arises from the long-range interactions introduced by the presence of polar amino acid residues. These interactions can be enhanced by dynamics specific to the gas phase environment, (i) large spatial fluctuations of the residues which are not constrained by solvent inertia,^{18,43} and (ii) large induced dipoles in residues resulting from the strong Coulomb fields originating on a nearby protonated site.

In the structural analysis of part I,¹⁰ fluctuations can result in (a) close proximity of the dye and Trp residue sufficient to form strong van der Waals interactions, and also in (b) proximity of the dye and Trp dipoles to both the Arg protonated site as well as the surrounding polar residues thus increasing electrostatic interactions. As a result, these fluctuations can affect the strength of the energy coupling, H_{12} , between reactant (Dye^*-Trp) and product ($\text{Dye}^--\text{Trp}^+$) electronic states, and also of interactions of the charge transfer state with the surrounding polar environment. It appears that the fluctuations of this peptide can play a role similar to solvent fluctuations in the Marcus formalism.

(b). *Ensemble Average of k_{et}* . The quenching data will be compared with a semiempirical electron transfer model based on the Marcus formulation. The primary emphasis will be to

compare the data with the temperature dependence predicted by the theoretical model in the high temperature limit. In this limit, both the Marcus and Jortner expressions for the transfer rate are similar in form and their dependence on parameters (λ , V_{12} , and ΔG_{act}) characterizing the reaction. Theoretical estimates of the implicit temperature dependence of these parameters shown in eqs 2–4 are beyond the scope of this analysis. These parameters will fluctuate at each temperature as the potential energies of both the reactant and product states vary with the fluctuations. However, we assume λ , V_{12} and ΔG_{act} introduce a weak temperature variation compared to the exponential dependence involving the activation energy and these parameters are taken to be constant in the following analysis.

Equation 4b includes the exponential factor $\exp(-\beta r_{\text{Dye-Trp}})$, which depends implicitly on the temperature through fluctuations of the Dye–Trp separation. This temperature dependence can be estimated by performing an ensemble average calculated over the MD trajectories for each starting structure at each temperature. The ensemble averaged electron transfer rate takes the form

$$\langle\langle k_{\text{et}}(T) \rangle\rangle \approx A \langle\langle \exp(-\beta r_{\text{Dye-Trp}}) \rangle\rangle_{t_i, \text{str}_i} \frac{1}{\sqrt{4\pi\lambda k_B T}} \exp(-\Delta G_{\text{act}}/k_B T) \quad (5)$$

where $A = (2\pi V_{12}^2)/\hbar$ is taken to be independent of temperature and the ensemble average of the electronic coupling factor is defined by

$$\begin{aligned} \langle\langle H_{12}^2 \rangle\rangle &= V_{12}^2 \langle\langle \exp(-\beta r_{\text{Dye-Trp}}) \rangle\rangle_{t_i, \text{str}_i} \\ &= \frac{\hbar}{2\pi} A \langle\langle \exp(-\beta r_{\text{Dye-Trp}}) \rangle\rangle_{t_i, \text{str}_i} \end{aligned} \quad (6)$$

The subscripts t_i and str_i indicate averages performed for each temperature. The t_i average is first calculated over the MD structures at each trajectory time step t_i for a given starting structure str_i , and the average is then taken over all starting structures. The activation energy, ΔG_{act} and A derived from fits will be assumed to represent an ensemble average of the theoretical value. The fits will determine ΔG_{act} and A for a specific value for λ as discussed below. This semiempirical fitting procedure is presently the most direct comparison we can perform between the temperature dependence of the electron transfer model and our experimental measurements.

4.2. Quenching Rate Data Fits. (a). *Ensemble Average of $r_{\text{Dye-Trp}}$.* It is helpful to consider the ensemble average of $r_{\text{Dye-Trp}}$ to show the mean and standard deviation of the distribution of the Dye–Trp separation. Figure 7a displays the ensemble average vs temperature that increases from 7.8 to 10.4 Å over the temperature range. A linear fit to all points is shown in Figure 7a and the uncertainty in the mean, $\sigma_{\text{Mean}} = \sigma_{\text{str}}/\sqrt{N}$, is shown at each temperature. Here $N = 5$ represents the number of starting structures (str) over which the averages are taken. These values are characterizing a distribution formed from all starting structures that will include contributions from many conformations. This will yield broad distributions that increase with temperature. Figure 8 shows the means and standard deviations (σ_{str}) of these distributions calculated in the form of cumulative histograms for temperatures 250–450 K. The individual peaks represent groups of similar conformations that yield significant contributions for $r_{\text{Dye-Trp}} < 6$ Å at each temperature. The distribution at 350 K is unique in the large

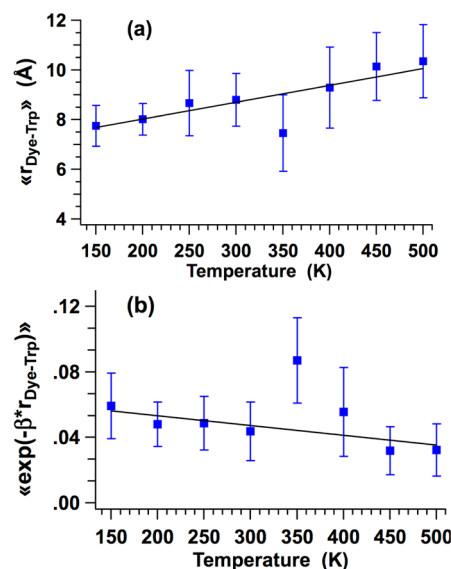


Figure 7. Averages (blue squares) vs temperature of (a) Dye–Trp separation $r_{\text{Dye-Trp}}$ and (b) exponential $\exp(-\beta r_{\text{Dye-Trp}})$. Error bars represent uncertainty of the mean calculated for the five starting structures. Linear fits to each ensemble average are indicated by the black lines.

peak located at smaller Dye–Trp separations and it is clear that this behavior produces the outlier in Figure 7a.

(b). *Ensemble Average of $\exp(-\beta r_{\text{Dye-Trp}})$.* The ensemble average of the exponential factor, $\langle\langle \exp(-\beta r_{\text{Dye-Trp}}) \rangle\rangle_{t_i, \text{str}_i}$ has been calculated for $\beta = 0.4 \text{ Å}^{-1}$ by the procedure discussed in section 4.1(b). Figure 7b displays a slow decrease with temperature as expected from variation of $\langle\langle r_{\text{Dye-Trp}} \rangle\rangle$ displayed in Figure 7a. A linear fit to all points is shown in Figure 7b with error bars representing the uncertainty of the mean calculated for the five starting structures. This fit was weighted by the mean uncertainty and yields an intercept of $y_0 = 0.07 \pm 0.02$ and slope $m = -(6 \pm 5) \times 10^{-5}$. The large standard deviation of the slope reflects the small slope and the uncertainty of the exponential factor. The exponential decreases with increasing temperature as the fluctuations increase the formation of larger Dye–Trp separations shown in Figure 7a. The average exponential factor decreases by only ~50% over the entire temperature range is a relatively minor contribution to the temperature dependence of the quenching rate. In our case, the compact polyproline bridge structure can contribute to the weak temperature dependence of the exponential. This slow variation of the exponential with temperature is independent of the value for the coefficient β .

(c). *β and λ Coefficients.* The value of β has not been determined in these experiments. The published literature that derives values of β for polyproline peptides in condensed phase is quite extensive. It has been shown that reliable estimates for this parameter require analyses to consider several interdependent phenomena. These include (i) the peptide conformations resulting from a distribution of trans and cis isomers in the peptide sequence^{14–16,44–46} which is an important factor determining the donor–acceptor separation;^{16,47,48} (ii) dependence of the donor–acceptor interaction on the dihedral angle between donor and acceptor planes;^{16,49,50} and (iii) the competition between electron transport through space and through bonds separating the donor–acceptor pair.^{14,45,47} Efforts to calculate and measure the electronic matrix element

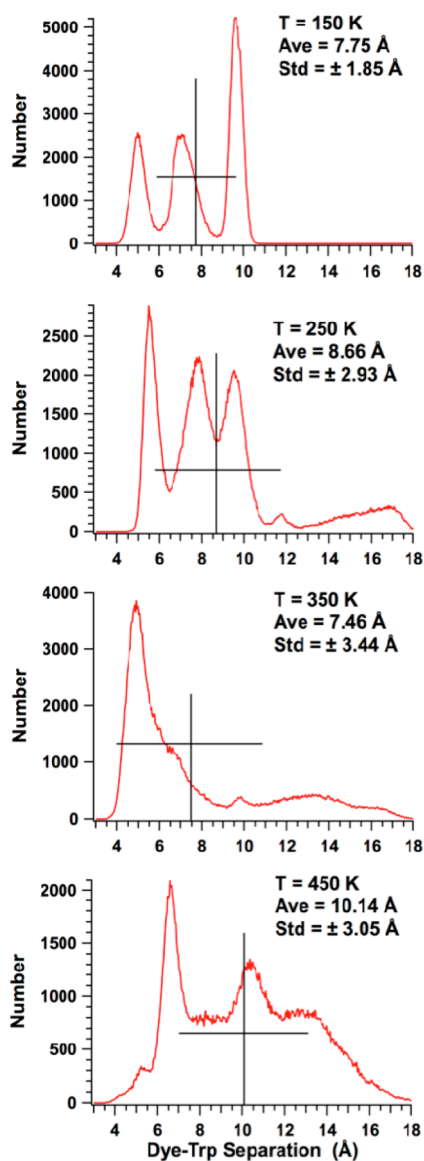


Figure 8. Cumulative histograms of the Dye–Trp separation over all starting structures at temperatures 150–450 K. The horizontal lines indicate 2σ , the standard deviation (Std) full width and vertical lines indicate the average of each distribution.

H_{12} directly have been applied^{16,51} to avoid the complexities introduced by these diverse issues.

These first measurements of desolvated peptides cannot rely on a large body of gas phase research to provide reliable estimates of undetermined parameters such as the β coefficient. However, it is clear that issues similar to those above could have a significant impact on the interpretation of gas phase data, in particular for peptides formed with a polyproline bridge. Further discussion of these gas phase issues has been included in the Supporting Information, section C. The starting structure cis–trans isomers and their consequences for the Dye–Trp separation are discussed more fully in section 3.3 of part I.

It is important to estimate the impact which the value of β (\AA^{-1}) has on the data fits. This has been performed by fitting the electron transfer model expressed in eq 5 to the quenching rate data for $\lambda = 1.6$ eV and values of β over the range $0.4 \leq \beta \leq 1.6$. This range was chosen from those observed in condensed phase measurements for polyproline bridges.^{16,47,48} Although β

will depend on the specific donor and acceptor species as well as the details discussed above, this coefficient range will serve to estimate the dependence on β .

A consequence of the weak temperature dependence of the average exponential factor is that the fits to eq 5 express a strong correlation between the value of β used to determine the fit value A_{fit} . The parameter A_{fit} simply compensates for the value of β , such that the value of the product

$$P_{A,\beta}(T) = A \langle \exp(-\beta r_{\text{Dye-Trp}}) \rangle \quad (7)$$

exhibits a similar temperature dependence for each (β , A_{fit}) pair. Figure 9 displays plots of $P_{A,\beta}(T)$ vs temperature for a set

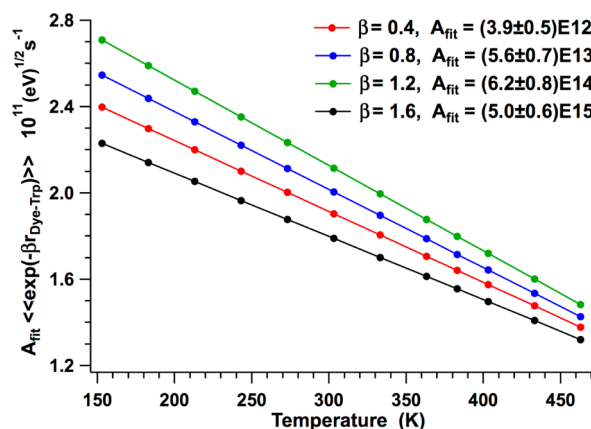


Figure 9. Product of the fit parameter A_{fit} and the ensemble average of the exponential $\exp(-\beta r_{\text{Dye-Trp}})$ is plotted vs temperature for β values of 0.4–1.6 \AA^{-1} . The weak variation of the product with β indicates the insensitivity of the fit to this undetermined parameter.

of four (β , A_{fit}) pairs. The standard deviation of the product is only 8.3% at 150 K and reduces to 4.1% at 500 K. This correlation provides an opportunity to avoid the uncertainties associated with an arbitrary choice of β and is an advantage in fitting the activation energy, ΔG_{act} , and estimating the average electronic coupling matrix element $\langle \langle H_{12} \rangle \rangle$ since both involve evaluation of the product $P_{A,\beta}(T)$. In the following analysis, we use a coefficient value of $\beta = 0.4 \text{ \AA}^{-1}$ which has been measured for photoinduced electron transfer in condensed phase measurements.¹³ The linear fit of the exponential factor in Figure 7b provides a smooth function of temperature to evaluate the exponential factor at each experimental temperature given by $\langle \langle \exp(-0.4 r_{\text{Dye-Trp}}) \rangle \rangle = 0.07 - (6 \times 10^{-5})T$.

Finally, the undetermined value for the reorganization energy will be taken as $\lambda = 1.6$ eV. Experimental values for the reorganization energy measured in condensed phase have been reported⁵² to fall within a range of $0.2 \text{ eV} \leq \lambda \leq 1.6$ eV. Larger λ will be shown below to be associated with values for the exothermicity that are consistent with the fit values for ΔG_{act} .

(d). **Data Fits.** Figure 10a displays the best fit to the quenching rate data obtained for parameter values $A_{\text{fit}} = 3.0 \pm 0.4 \times 10^{12} \text{ s}^{-1}$ and $\Delta G_{\text{act}} = 0.290 \pm 0.004$ eV. The error bars in Figure 10a have been calculated to reflect the uncertainty introduced by the ensemble averaging arising from the calculation of the exponential factor. The uncertainty in k_q , δk_q , can be related to that of the average $\langle \langle \exp(-\beta r_{\text{Dye-Trp}}) \rangle \rangle$ by using eq 5 to write $\delta k_q/k_q = \delta \langle \exp(\beta r_{\text{DT}}) \rangle / \langle \exp(\beta r_{\text{DT}}) \rangle$. Here $\delta \langle \exp(\beta r_{\text{DT}}) \rangle$ is just the σ_{Mean} of the average $\langle \langle \exp(-\beta r_{\text{Dye-Trp}}) \rangle \rangle$. The lifetime, τ , is calculated from eq 1 using τ_0 given in section 3.1 and the quenching rate determined by the

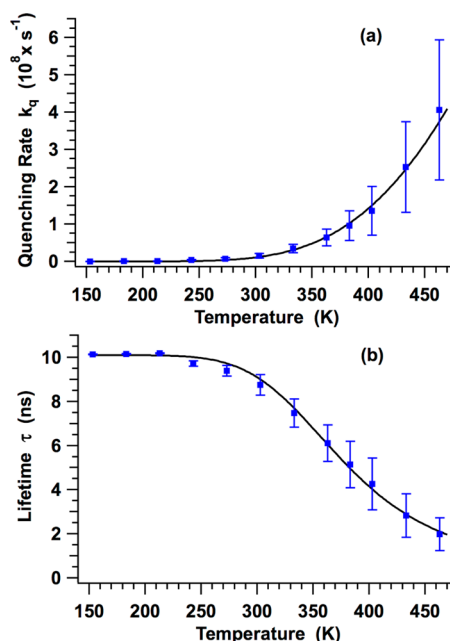


Figure 10. (a) Fit of the electron transfer rate model given in eq 5 to the quenching rate vs temperature data for peptide sequence DyeX-Pro₄-Arg⁺-Trp. Data is shown by blue squares and the fit by the solid black curve. (b) Calculated lifetimes (black curve) using the fit of the electron transfer rate model in eq 1 and the measured lifetime data (blue squares) vs temperature. The error bars are derived in the text from the uncertainty of the mean calculated for the five starting structures.

fit. The calculated and measured lifetimes are compared in Figure 10b where the error bars are the uncertainty in τ given by $\delta\tau = \tau^2\delta k_q$. The fits in Figure 10 indicate that the temperature dependence of the quenching rate is consistent with the dependence predicted by the Marcus model¹³ for electron transfer expressed by eq 5b. It remains to be demonstrated below that the fit values A_{fit} and ΔG_{act} yield physically reasonable values for the electronic coupling, H_{12} , and the reaction exothermicity, ΔG .

(e). *Energy Parameters H_{12} and ΔG . Electronic Matrix Element H_{12} .* Equation 2 is the starting point to calculate the nonadiabatic electron transfer rate involving a transition from an eigenstate to a dense continuum of eigenstates as the result of a perturbation. A discussion of both adiabatic and nonadiabatic electron transfer is presented in review articles.^{13,40} The nonadiabatic approach is applied to calculate the electron transfer rate when H_{12} , the matrix element of the coupling interaction, satisfies the condition $H_{12} \ll k_B T$.⁵³ We have calculated electron transfer for the peptide under discussion assuming a weak electronic interaction so that the nonadiabatic formalism is appropriate. However, Figures 3 and 8 show that the Dye-Trp trajectories have significant contributions for separations $< 6 \text{ \AA}$ which suggest that the use of a nonadiabaticity model requires further justification. The matrix element will be estimated from the value of A_{fit} and then will be compared with values available in the published literature.

Calculation of $\langle\langle H_{12}^2 \rangle\rangle$ involves the fit parameter A_{fit} and the ensemble average of the exponential factor vs temperature as shown in eq 1. The data shown in Figure 7b are used for the exponential factor and we estimate the average matrix element by approximating $\langle\langle H_{12} \rangle\rangle \approx (\langle\langle H_{12}^2 \rangle\rangle)^{1/2}$. The resulting

matrix element $\langle\langle H_{12} \rangle\rangle$ values are plotted vs temperature in Figure 11. The uncertainty in $\langle\langle H_{12}^2 \rangle\rangle$ can be related to the

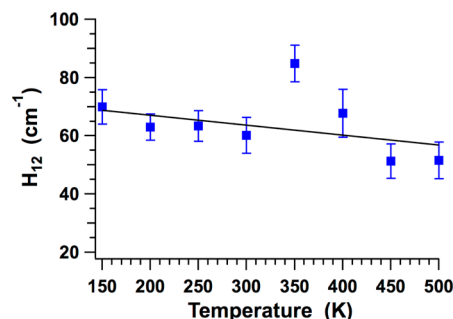


Figure 11. Ensemble average of the electronic matrix element H_{12} vs temperature. This calculation is derived from the fit parameter A_{fit} as described in text. The error bars are derived from the ensemble average of the exponential factor as described in text.

σ_{Mean} of the average $\langle\langle \exp(-\beta r_{\text{Dye-Trp}}) \rangle\rangle$ by using eq 6 to write $\delta\langle\langle H_{12}^2 \rangle\rangle / \langle\langle H_{12}^2 \rangle\rangle = \delta\langle\langle \exp(\beta r_{\text{DT}}) \rangle\rangle / \langle\langle \exp(\beta r_{\text{DT}}) \rangle\rangle$. The σ_{Mean} of $\langle\langle H_{12} \rangle\rangle$ shown in Figure 11 can be derived from $\delta\langle\langle H_{12}^2 \rangle\rangle$ and is given by $\delta\langle\langle H_{12} \rangle\rangle / \langle\langle H_{12} \rangle\rangle = \delta\langle\langle \exp(\beta r_{\text{DT}}) \rangle\rangle / 4\langle\langle \exp(\beta r_{\text{DT}}) \rangle\rangle$. The values of $\langle\langle H_{12} \rangle\rangle$ are less than 90 cm^{-1} (including the outlier) so that $\langle\langle H_{12} \rangle\rangle \ll k_B T$ over the experimental temperature range from which we conclude that the non-adiabatic model was appropriate.

It is interesting to compare the values for $\langle\langle H_{12} \rangle\rangle$ calculated above from fit parameters to those matrix elements resulting from measurements of photoinduced electron transfer in condensed phase.¹⁶ In each case, the conformer structures are responsible for ensemble averaged electron transfer rates and also average matrix elements. In our measurements these conformer structures arise from large-scale fluctuations of the dye and tryptophan side chain. In the condensed phase measurements the dynamics are diffusion limited and different conformer structures result from different cis-trans combinations of proline residues.

In the condensed phase measurements, Pyr (pyrene-1-sulfonyl) served as the acceptor covalently attached at the N terminus of a polyproline peptide and the electron donor was DMPD (*N,N*-dimethyl-1,4-phenylenediamine) placed at the C terminus. A fluorescence spectrum from the electron transfer state exhibited a red-shifted emission band that enabled calculations⁵⁴ of the coupling energy H_{12} for various conformer structures of Pyr-Pro_{*n*}-DMPD. We have used these calculations to estimate an average $\langle H_{12} \rangle$ weighted by the free energy of the conformer, for the 4 lowest energy structures of $n = 2$ and the 6 lowest energy structures of $n = 3$. This provides an order of magnitude estimate for $\langle H_{12} \rangle$ to compare with the range of values shown in Figure 11. This yields values of $\langle H_{12} \rangle \approx 100 \text{ cm}^{-1}$ for both $n = 2$ and $n = 3$, which are comparable to the range of values in Figure 11. Several points are interesting to note. The variation of conformer H_{12} values¹⁶ indicated an exceptionally strong dependence on structure. Conformers having the largest H_{12} for both $n = 2$ and 3 correspond to structures for which the Pyr-DMPD rings have increased π - π ring interactions for center-center separations expected for strong van der Waals interactions. Similar donor-acceptor configurations were identified in the analysis of photoinduced electron transfer measured with coumarin dye acceptors and organic solvent donors.⁵⁵ Part I¹⁰ also discussed the importance of such donor-acceptor orientations in the structural dynamics

of the DyeX-Pro₄-Arg⁺-Trp peptide. Although the electronic matrix elements will depend on the specific donor/acceptor molecules, the strong dependence on the donor–acceptor proximity and orientation¹⁶ in both condensed and gas phase electron transfer is consistent with the comparable values of $\langle H_{12} \rangle$ shown in Figure 11.

Exothermicity. ΔG values for the exothermicity can be calculated from the fit value of the activation energy ΔG_{act} using eq 4a which yields $\Delta G = -\lambda \pm 2(\lambda \Delta G_{\text{act}})^{1/2}$. Figure 12 plots the

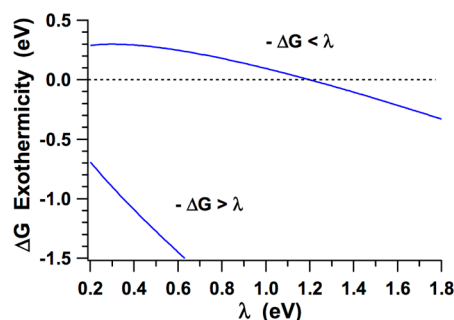


Figure 12. Exothermicity of the electron transfer reaction, ΔG , vs reorganization energy λ derived from the fit parameters of the electron transfer model as described in the text.

resulting ΔG vs λ for both solution branches, $-\Delta G < \lambda$ and $-\Delta G > \lambda$. We note that exothermic reactions, $\Delta G < 0$, can occur for both branches, however, the intramolecular environment in the desolvated, protonated peptide arising from electrostatic and polarization interactions would probably lead to larger values of λ , and in this case, the $-\Delta G < \lambda$ branch would be preferred. A rough estimate⁵³ for λ yields values ~ 1.5 eV. The estimates for the $-\Delta G < \lambda$ branch indicate that exothermic values of ΔG fall in the range $0 \leq -\Delta G \leq 0.25$ eV. As indicated in ref 52, this range of values for ΔG is consistent with quenching rates of 10^7 to 10^8 s⁻¹ for ΔG_{act} of ~ 0.3 eV and Dye–Trp separations of 4–6 Å. Consequently, the exothermicity energies estimated from the fit parameter ΔG_{act} are reasonable values for the range of quenching rates measured for the gas phase peptide.

The MD calculations provide an opportunity to estimate the temperature dependence of ΔG by calculating the difference in the electronic energies of the reactant and product states. This estimate of ΔG was calculated as the energy difference between the reactant state sequence DyeX^{*}-Pro₄-Arg⁺-Trp of the peptide excited state and the product state sequence DyeX⁻-Pro₄-Arg⁺-Trp⁺ of the electron transfer state. The atomic positions in the reactant state are taken to be identical to the ground state and these states are separated in energy by $h\nu$, the photon energy. For the purpose of estimating a lower bound to the exothermicity, these same atomic positions will be used to calculate the electrostatic and polarization energies that increase the binding energy of the product state. This estimate assumes that the equilibrium geometry of the product state will lead to a more compact structure having greater binding. The calculation of ΔG at each structure fluctuation determined by the MD calculation provides a basis for understanding how the intramolecular interactions increase the probability for electron transfer.

Rhem and Weller⁵⁶ used similar energy calculations to predict the possibility for electron transfer in condensed phase. Here, we formulate an analysis appropriate for desolvated peptide ions that includes both electrostatic and polarization

contributions. In the absence of solvent, contributions due to changes in entropy are expected to be small¹³ and ΔG is estimated by the sum of three enthalpies

$$\Delta G = \Delta E_0 + \Delta E_{\text{Coul}} + \Delta E_{\text{Chrg-Dip}} \quad (8)$$

The parameters used in calculating the terms in eq 8 have been discussed previously⁷ and equations for the individual terms are discussed in the Supporting Information, Section D. ΔE_0 is similar to the expression derived by Rhem and Weller for electron transfer in condensed phase and by Jortner⁴² in discussions of transfer in gas phase molecules and is given by

$$\Delta E_0 = \left[\text{IP}_{\text{Trp}} - \text{EA}_{\text{Dye}} - \frac{e^2}{\epsilon r_{\text{Dye-Trp}}} \right] - E_{00} \quad (9)$$

This term depends on the tryptophan ionization potential, IP_{Trp} , the dye electron affinity, EA_{Dye} , the Coulomb interaction of the charge separated pair, Dye⁻ and Trp⁺, and the energy of the dye excited state, E_{00} . ΔE_{Coul} includes the Coulomb interactions between Arg⁺-Trp⁺, and Arg⁺-Dye⁻ resulting from the arginine protonation site. The terms in $\Delta E_{\text{Chrg-Dip}}$ represent interactions of the charge-separated pair with the steady state dipoles and polarizabilities of the peptide side chains. These dipole moments and polarizabilities have been obtained from density functional calculations⁵⁷ and rotation of the steady state dipoles has been taken into account.⁵⁸ The side chain separations in each of the contributions of eq 8 are obtained from the MD calculations. The background dielectric constant⁵⁹ $\epsilon = 1.4$ is included to represent shielding of the intramolecular electric fields and the effects of dipole fields not included in this formulation.

In principle, the energies represented by $\Delta E_{\text{Chrg-Dip}}$ are included in the AMOEBA algorithm by considering the polarizability of each atom and this basis provided a more reliable calculation of the conformational fluctuations. However, it seemed a more intuitive approach, adequate for the purposes of estimating ΔG to simply treat the individual side chains and the dye. These calculations assume integer charges on the formally charged sites; do not include the backbone dipoles and polarizability; and ignore van der Waals and dipole–dipole interactions.

Some of the more interesting results of these calculations can be drawn from the plots of ΔG vs Dye–Trp separation shown in Figure 13 and the trajectories in Figure 14. Figure 13 indicates that the number of structures that provide exothermicity ($\Delta G < 0$) increases with increasing temperature. This increase occurs as the number of peptide structures that result in smaller values of the Dye–Trp separation increases with temperature from 200 to 400 K depending on the starting structure. As the temperature increases, only starting structures 2 and 7 exhibit monotonic increases in exothermic conformers. Other starting structures exhibit relatively minor contributions to exothermic conformers possibly as a result of localization in deeper well depths. In particular, starting structure 4 has a polypeptide bridge composed of all trans isomers which will result in a bridge structure having a longer length, thus reducing electrostatic contributions (see Supporting Information, section C). The shape of the conformer distributions in Figure 13 exhibit distinct curvature at smaller Dye–Trp separations and exhibit a *linear* dependence when ΔG is plotted vs $1/(r_{\text{Dye-Trp}})^4$ as shown in Figure S4, Supporting Information. Consequently, Figure 13 exhibits increasing importance of charge-induced

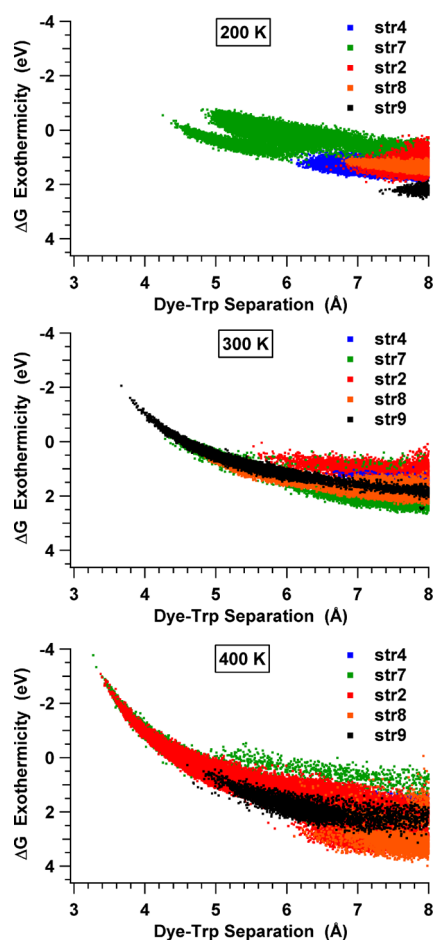


Figure 13. Exothermicity of the electron transfer reaction, ΔG , vs the Dye–Trp separation calculated from MD trajectories as described in the text. The panels show calculations at temperatures covering the experimental range. Each panel is composed of points for all starting structures which are color coded according to the legend. Each point corresponds to the structure at an MD time step for which the exothermicity and separation distance are calculated.

dipole interactions between the Dye^- and Trp^+ that are proportional to $1/(r_{\text{Dye-Trp}})^4$.

Figure 14 shows trajectories calculated for each contribution to ΔG expressed in eq 7. These trajectories at 400 K for starting structure 2 show that exothermicity ($\Delta G < 0$) occurs only for Dye–Trp separations of $\sim 4\text{--}6$ Å for which values of $\Delta E_0 + \Delta E_{\text{Chrg-Dip}}$ are greater than ΔE_{Coul} . This example suggests that the charge-dipole interactions can be sufficient at small Dye–Trp separations to produce the exothermicity required for electron transfer reactions.

The effects of strong, *intramolecular* electric fields on electron transfer in condensed phase measurements were previously demonstrated in dichromophoric α -helical peptides.⁶⁰ Axial fields of the macro dipole in alpha helices were estimated on the basis of vacuum electrostatics to reach values of $\sim 10^7$ V/cm. Fields of this magnitude were shown to significantly modify the exothermicity as well as the activation energy of an observed electron transfer reaction. In the desolvated peptide measurements under consideration here, the intramolecular Coulomb fields associated with the charge-separated pair, Dye^- and Trp^+ , approach 10^8 V/cm during the close encounters of $\sim 4\text{--}6$ Å resulting from spatial fluctuations.⁷ Given the absence of shielding in this strong field environment, it is probably not

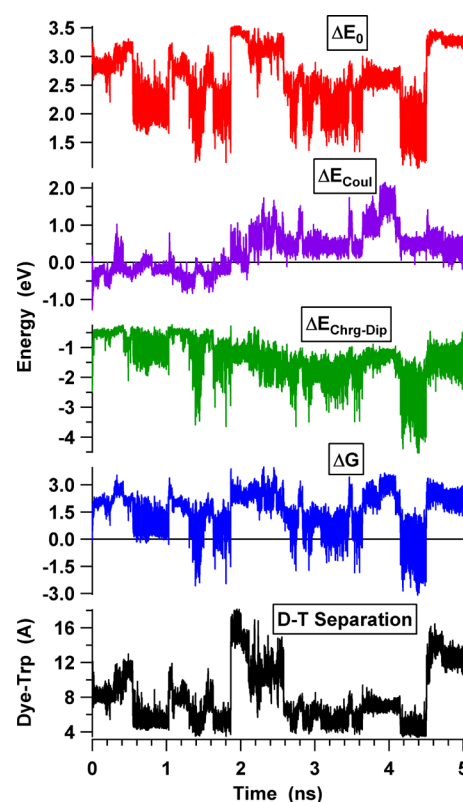


Figure 14. Energy components ΔE_0 (red), ΔE_{Coul} (purple), $\Delta E_{\text{Chrg-Dip}}$ (green), ΔG (blue), and the Dye–Trp separation (black) as a function of time, taken from the MD trajectory starting from structure str2 at 400 K.

surprising that the charge-induced dipole interactions make significant contributions to the estimated electron transfer exothermicity. Quenching rate data also has been reported⁷ for desolvated peptide sequences $\text{Dye-Trp-Pro}_n\text{-Arg}^+$. These data demonstrated that electrostatic interactions involving strong intramolecular fields significantly influenced the quenching process. A short summary of these data is included in the Supporting Information, section A.

5. SUMMARY AND CONCLUSIONS

This paper compares the temperature dependence of the experimental fluorescence quenching rate for a desolvated peptide with the dependence predicted by the Marcus model¹³ for the rate of electron transfer. The analysis presented here also relies on the interpretation of electron transfer in desolvated biomolecules by Jortner.⁴²

Dynamics simulations have been performed to investigate the temperature dependence of the conformational fluctuations in order to identify structural trends that increase the rate of electron transfer reactions. The uncertainty associated with identifying such trends was reduced by choice of the peptide sequence in which only the dye and tryptophan side chain exhibited fluctuations among an ensemble of different conformations. MD trajectories identified small amplitude fluctuations of the Dye–Trp separation that are most likely related to smaller changes in orientation associated with torsional motions about the $(C_\alpha\text{--}C_\beta)$ and $(C_\beta\text{--}C_\gamma)$ bonds of the tryptophan residue as well as about the (C--C) bonds of the CH_2 chain in the dye linker. Large-scale fluctuations of the Dye–Trp separation corresponding to collective motions of the

dye and tryptophan side chain lead to changes in conformation that are stable for nanosecond time scales. These large amplitude fluctuations were most clearly correlated with torsional dynamics at lower temperatures and were responsible for changes in the Dye–Trp separation that increased the probability of electron transfer. As a result of these MD analyses, through-space interactions are assumed to dominate this transfer. For example, conformations are observed in which the center-to-center separations between the dye and tryptophan side chain are ca. 4–6 Å leading to van der Waals interactions and wave function overlap that enhances the electronic coupling interaction required for electron transfer. The temperature dependence of these fluctuations suggests that increasing temperature enables a conformation to surmount localization within the relatively deep electrostatic wells in order to sample and arrive at structures more probable for electron transfer. Note that although only five different starting structures were used in these MD calculations, the number of different conformations forming the ensemble averages were 1–2 orders of magnitude greater in number. The MD calculations suggest that the dynamics responsible for driving these fluctuations were the torsional motions. These are relatively low frequency modes, ν_T , and are assumed to be the important frequencies involved in electron transfer reactions. Consequently, the high temperature regime, $k_B T \gg h\nu_T$, satisfies the assumption of classical vibrations applied in the derivation of the Marcus model for electron transfer.

Fitting the experimental temperature dependence of the quenching rate to the Marcus model included calculating an ensemble average of the exponential in the Dye–Trp center-to-center separation using trajectories provided by the MD simulation. It was found that the implicit temperature dependence of this average was significantly weaker than any other temperature dependence in the Marcus model. Average of the Dye–Trp separations do increase at higher temperatures as a result of increased fluctuations, but averaging over starting structures includes structures that are strongly localized on the potential energy surface. The fitting procedure yields very close fits between the quenching data and the Marcus model, displaying a temperature dependence dominated by the exponential in the activation energy. A more critical result of these fits is that the electronic coupling matrix element, H_{12} , and the transfer reaction exothermicity, ΔG , derived from the fitting parameters correspond to physically reasonable values which are comparable to previously determined values in condensed phase measurements of similar polyproline peptides.

In principle, current parallel computing technology could be applied to calculate a more reliable ensemble average by increasing the number of starting structures. However, it should be recognized that variations in the MD trajectories for different starting structures depend in large part on the degree of localization introduced by deep wells resulting from electrostatics and polarization. These are intrinsic characteristics of the desolvated, protonated peptides and are in fact why these species are of interest. The AMOEBA force field provides a reliable model of these intramolecular interactions that helps to observe and evaluate their contribution to the dynamics.

There are unresolved issues related to the electron transfer details in the desolvated peptide analysis that are clearly well beyond the scope of the paper's analysis. These include (i) a more thorough analysis of the cis–trans isomer distribution in the proline bridging chain, (ii) a more reliable approach to identify unknown parameters such as β and λ , and (iii) an

extension of calculations to analyze the product state as well as the reactant state. However, we believe the results of this initial study do lend serious support to establish electron transfer as the physical basis of the fluorescence quenching process in the desolvated peptide studied. The similarities between the temperature dependence obtained from this peptide and other peptide sequences studied,⁷ as well as the Trp–cage protein⁸ and vancomycin–peptide noncovalent complex⁸ suggest that the interpretation based on electron transfer is not limited to the peptide dynamics analyzed in this paper. Analyses of these additional biomolecules are currently being performed using methods similar to those described here. The Trp–cage protein and vancomycin–peptide noncovalent complex are particularly interesting in that the fluorescence quenching data is shown to be useful to interpret changes in conformation due to site specific mutations which alter intramolecular interactions.

Experimental directions are planned to continue quenching measurements in biomolecules (i) related to specific changes in conformation of secondary structure, (ii) conformational change induced by metal ligands, and (iii) the use of donor and acceptor species having a high probability to yield fluorescence emitted by the electron transfer state.

■ ASSOCIATED CONTENT

Supporting Information

Data and analysis related to (A) quenching data for peptide sequences, Dye–Trp–Pro_n–Arg⁺; (B) peptide structures calculated with the AMOEBA force field; (C) issues related to the exponential coefficient β ; and (D) calculation for the exothermicity ΔG from MD trajectories. This material is available free of charge via the Internet at <http://pubs.acs.org>.

■ AUTHOR INFORMATION

Corresponding Author

*E-mail: parks@rowland.harvard.edu Phone: (617) 497-4653. Fax: (617) 497-4627.

Notes

The authors declare no competing financial interest.

■ ACKNOWLEDGMENTS

We gratefully acknowledge helpful discussions with Dr. James Foley (Rowland), Dr. Michael Burns (Rowland), Dr. Alan Stern (Rowland) and Dr. Abraham Szoke. We acknowledge the generous financial support by the National Science Foundation (Grant CHE-0962680) and by The Rowland Institute at Harvard during the early stage of this research.

■ REFERENCES

- (1) (a) Danell, A.; Parks, J. H. *Int. J. Mass Spectrom.* **2003**, *229*, 35–45. (b) Danell, A. S.; Parks, J. H. *J. Am. Soc. Mass Spectrom.* **2003**, *14*, 1330–1339.
- (2) Dashtiev, M.; Azov, V.; Frankevich, V.; Scharfenberg, L.; Zenobi, R. *J. Am. Soc. Mass Spectrom.* **2005**, *16*, 1481–1487.
- (3) Francis O. Talbot, F. O.; Anthony Rullo, A.; Huihui Yao, H.; Jockusch, R. A. *J. Am. Chem. Soc.* **2010**, *132*, 16156–16164.
- (4) Iavarone, A. T.; Parks, J. H. *J. Am. Chem. Soc.* **2005**, *127*, 8606–8607; (b) *129*, 6726–6735.
- (5) Iavarone, A. T.; Meinen, J.; Schulze, S.; Parks, J. H. *Int. J. Mass Spectrom.* **2006**, *253*, 172–180.
- (6) Iavarone, A. T.; Patriksson, A.; Van der Spoel, D.; Parks, J. H. *J. Am. Chem. Soc.* **2007**, *129*, 6726–6735.
- (7) Shi, X.; Duft, D.; Parks, J. H. *J. Phys. Chem. B* **2008**, *112*, 12801–12815.

- (8) Shi, X.; Parks, J. H. *J. Am. Soc. Mass Spectrom.* **2010**, *21*, 707–718.
- (9) Iavarone, A. T.; Duft, D.; Parks, J. H. *J. Phys. Chem. A* **2006**, *110*, 12714–12727.
- (10) Semrouni, D.; Clavaguera, C.; Ohanessian, G.; Parks, J. H. *J. Phys. Chem. B* **2013**, DOI: 10.1021/jp3078375.
- (11) Marcus, R. A. *J. Chem. Phys.* **1956**, *24*, 966–978.
- (12) Marcus, R. A. *Annu. Rev. Phys. Chem.* **1964**, *15*, 155–196.
- (13) Marcus, R. A.; Sutin, N. *Biochim. Biophys. Acta* **1985**, *811*, 265–322.
- (14) Isied, S. S.; Ogawa, M. Y.; Wishart, J. F. *Chem. Rev.* **1992**, *92*, 381–394.
- (15) Isied, S. S. In *Principles of Electron-Transfer Reactions: Application in Inorganic and Organometallic Chemistry and Biology*; Isied, S. S., Ed.; Advances in Chemistry Series 253; American Chemical Society: Washington, DC, 1997.
- (16) Issa, J. B.; Salameh, A. S.; Castner, E. W., Jr.; Wishart, J. F.; Isied, S. S. *J. Phys. Chem. B* **2007**, *111*, 6878–6886 and references therein..
- (17) Felker, P. M.; Syage, J. A.; Lambert, W. R.; Zewail, A. H. *Chem. Phys. Lett.* **1982**, *92*, 1–3.
- (18) Syage, J. A.; Felker, P. M.; Zewail, A. H. *J. Chem. Phys.* **1984**, *81*, 2233–2256.
- (19) van Dantzig, N. A.; Shou, H.; Alfano, J. C.; Yang, N. C.; Levy, D. H. *J. Chem. Phys.* **1994**, *100*, 7068–7078.
- (20) Jortner, J.; Bixon, M.; Wegewijs, B.; Verhoeven, J. W.; Rettschnick, R. P. H. *Chem. Phys. Lett.* **1993**, *205*, 451–455.
- (21) Verhoeven, J. W.; Wegewijs, B.; Scherer, T.; Rettschnick, R. P. H.; Warman, M.; Jager, W.; Schneider, S. J. *Phys. Org. Chem.* **1996**, *9*, 387–397.
- (22) Rasmussen, T. D.; Ren, P.; Ponder, J. W.; Jensen, F. *Int. J. Quantum Chem.* **2007**, *107*, 1390–1395.
- (23) Yue, S.; Wu, C.; Ponder, J. W.; Pengyu, R. *J. Comput. Chem.* **2011**, *32*, 967–977.
- (24) Ponder, J. W. *Tinker, Software Tools for Molecular Design*, Version 5.1, 2010. <http://dasher.wustl.edu/tinker/>.
- (25) Stone, A. J.; Alderton, M. *Mol. Phys.* **1985**, *56*, 1047–1064.
- (26) Stone, A. J. *Distributed Multipole Analysis for Gaussian Wavefunctions*, version 2.2.03, 2005–2007. <http://www-stone.ch.cam.ac.uk/pub/gdma/download.php>.
- (27) Counterman, A. E.; Clemmer, D. E. *J. Phys. Chem. B* **2004**, *108*, 4885–4898.
- (28) Wriggers, W.; Chakravarty, S.; Jennings, P. A. *Biopolymers* **2005**, *80*, 736–746.
- (29) Pettersen, E. F.; Goddard, T. D.; Huang, C. C.; Couch, G. S.; Greenblatt, D. M.; Meng, E. C.; Ferrin, T. E. *J. Comput. Chem.* **2004**, *25*, 1605–1612.
- (30) Meng, E. C.; Pettersen, E. F.; Couch, G. S.; Huang, C. C.; Ferrin, T. E. *BMC Bioinformatics* **2006**, *7*, 339–348.
- (31) Swaminathan, S.; Ichiye, T.; van Gunsteren, W.; Karplus, M. *Biochemistry* **1982**, *21*, 5230–5241.
- (32) Henry, E. R.; Hochstrasser, R. M. *Proc. Natl. Acad. Sci. U.S.A.* **1987**, *84*, 6142–6146.
- (33) Rizzo, T. R.; Park, Y. D.; Peteanu, L. A.; Levy, D. H. *J. Chem. Phys.* **1986**, *84*, 2534–2541.
- (34) Rizzo, T. R.; Park, Y. D.; Levy, D. H. *J. Chem. Phys.* **1986**, *85*, 6945–6951.
- (35) Bersohn, R.; Even, U.; Jortner, J. *J. Chem. Phys.* **1984**, *80*, 1050–1058.
- (36) Hager, J.; Wallace, S. C. *J. Phys. Chem.* **1983**, *87*, 2121–2127.
- (37) Hays, T. R.; Henke, W. E.; Selzle, H. L.; Schlag, E. W. *Chem. Phys. Lett.* **1983**, *97*, 347–351.
- (38) Rouille, G.; Arold, M.; Staicu, A.; Henning, T.; Huisken, F. *J. Phys. Chem. A* **2009**, *113*, 8187–8194.
- (39) Doster, W.; Cusack, S.; Petry, W. *Nature* **1989**, *337*, 754–756.
- (40) Barbara, P. F.; Meyer, T. J.; Ratner, M. A. *J. Phys. Chem.* **1996**, *100*, 13148–13168.
- (41) Jortner, J. *J. Chem. Phys.* **1976**, *64*, 4860–4867.
- (42) Jortner, J.; Bixon, M.; Heitele, H.; Michel-Beyerle, M. E. *Chem. Phys. Lett.* **1992**, *197*, 131–135.
- (43) Wang, Y.; Crawford, M. C.; Eienthal, K. B. *J. Am. Chem. Soc.* **1982**, *104*, 5874–5878.
- (44) Isied, S. S.; Vassilian, A. *J. Am. Chem. Soc.* **1984**, *106*, 1732–1736.
- (45) Sneddon, S. F.; Brooks, C. L., III. *J. Am. Chem. Soc.* **1992**, *114*, 8220–8225.
- (46) Doose, S.; Neuweiler, H.; Barsch, H.; Sauer, M. *Proc. Natl. Acad. Sci. U.S.A.* **2007**, *104*, 17400–17405.
- (47) Bobrowski, K.; Holcmaqt, J.; Poznaiski, J.; Ciurak, M.; Wierzbowski, K. L. *J. Phys. Chem.* **1992**, *96*, 10036–10043.
- (48) Mishra, A. K.; Chandrasekar, R.; Faraggi, M.; Klapper, M. H. *J. Am. Chem. Soc.* **1994**, *116*, 1414–1422.
- (49) Cave, R. J.; Siders, P.; Marcus, R. A. *J. Phys. Chem.* **1986**, *90*, 1436–1444 and references therein..
- (50) Helms, A.; Heiler, D.; McLendon, G. *J. Am. Chem. Soc.* **1991**, *113*, 4325–4327.
- (51) Issa, J. B.; Krogh-Jespersen, K.; Isied, S. S. *J. Phys. Chem. C* **2010**, *114*, 20809–20812.
- (52) Moser, C. C.; Page, C. C.; Dutton, P. L. *Philos. Trans. R. Soc., London, Ser. B* **2006**, *361*, 1295–1305.
- (53) Closs, G. L.; Miller, J. R. *Science* **1988**, *240*, 440–447.
- (54) (a) Cave, R. J.; Newton, M. D. *Chem. Phys. Lett.* **1996**, *249*, 15–19. (b) Rust, M.; Lappe, J.; Cave, R. J. *J. Phys. Chem. A* **2002**, *106*, 3930–3940.
- (55) Castner, E. W., Jr.; Kennedy, D.; Cave, R. J. *J. Phys. Chem. A* **2000**, *104*, 2869–2885.
- (56) Rehm, D.; Weller, A. *Isr. J. Chem.* **1970**, *8*, 259–271.
- (57) Millefiori, S.; Alparone, A.; Millefiori, A.; Vanella, A. *Biophys. Chem.* **2008**, *132*, 139–147.
- (58) Eyring, H.; Henderson, D.; Stover, B. J.; Eyring, E. M. *Statistical Mechanics and Dynamics*, 2nd ed.; John Wiley and Sons: New York, 1982.
- (59) Schnier, P. D.; Gross, D. S.; Williams, E. R. *J. Am. Chem. Soc.* **1995**, *117*, 6747–6757.
- (60) (a) Galoppini, E.; Fox, M. A. *J. Am. Chem. Soc.* **1996**, *118*, 2299–2300. (b) Galoppini, E.; Fox, M. A. *J. Am. Chem. Soc.* **1997**, *119*, 5277–5285.